
"Teaching Independent Parts Separately" (TIPS-GAN) : Improving Accuracy and Stability in Unsupervised Adversarial 2D to 3D Human Pose Estimation

Peter Hardy*

Vision Learning and Control Research Group
University of Southampton
Hampshire, UK
p.t.d.hardy@soton.ac.uk

Srinandan Dasmahapatra

Vision Learning and Control Research Group
University of Southampton
Hampshire, UK
sd@ecs.soton.ac.uk

Hansung Kim

Vision Learning and Control Research Group
University of Southampton
Hampshire, UK
h.kim@soton.ac.uk

Abstract

We present TIPS-GAN, a new approach to improve the accuracy and stability in unsupervised adversarial 2D to 3D human pose estimation. In our work we demonstrate that the human kinematic skeleton should not be assumed as one spatially dependent structure. In fact, we believe when a full 2D pose is provided during training, there is an inherent bias learned where the 3D coordinate of a keypoint is spatially codependent on the 2D locations of all other keypoints. To investigate our theory we follow previous adversarial approaches but trained two generators on spatially independent parts of the kinematic skeleton, the torso and the legs. During our study we find that improving self-consistency is key to lowering the evaluation error and therefore introduce new consistency constraints within the standard adversarial cycle. We then produced a final TIPS model via knowledge distillation which can predict the 3D coordinates for the entire 2D pose with improved results. Furthermore we help address the question left unanswered in prior adversarial learning papers of how long to train for a truly unsupervised scenario. We show that two independent generators training adversarially can hold a minimum error against a discriminator for a longer period of time than that of a solo generator which will diverge due to the adversarial network becoming unstable. TIPS decreases the average error by 18% when compared to that of a baseline solo generator. TIPS improves upon other unsupervised approaches while also performing strongly against supervised and weakly-supervised approaches during evaluation on both the Human3.6M and MPI-INF-3DHP dataset. **Code and weights of our model will be made available**

*<https://www.ecs.soton.ac.uk/people/ptdh1c20>

1 Introduction

The ability to generate accurate 3D human skeletons from images and video has extensive applications in security, human-robot interaction, interactive media and healthcare [46] [10] [25]. Estimating a 3D pose from a single monocular image however, is an ill-posed inverse problem as multiple different 2D poses can correspond to the same 3D pose. Additionally, many state of the art 3D human pose estimation (HPE) approaches [26] [5] [50] [17] [28] [24] [9] [34] [44] [53], utilise ground truth 3D pose data during training. The actual acquisition of 3D pose data however, is both time-consuming and expensive, meaning that the most popular 3D datasets contain few subjects, within a controlled environment and performing a limited number of actions. Unsupervised adversarial approaches [6] [19] [52] have sought to remedy this by exploiting the abundance of readily available 2D image and video data of humans. Through the use of self or temporal consistency and a 2D pose discriminator, they help to reduce the barrier of entry for 3D HPE while improving generability to in the wild scenarios. However, most unsupervised approaches perform sub-par during evaluation on 3D HPE datasets when compared against their supervised counterparts. Our research aims to reduce this discrepancy and address what we believe is a flaw in all adversarial 2D to 3D HPE models, that the human kinematic skeleton should be treated as one independent structure.

When a model is trained on an entire 2D pose to predict 3D coordinates we believe a bias is learnt, where the 3D coordinate of a keypoint is spatially codependent on all the other keypoints 2D coordinates. Meaning the prediction for the left wrists 3D coordinate will contain some component corresponding to the 2D coordinates of the right ankle, right knee, etc. We grant that overtime a good model should learn suitable weights for features which are important during prediction, observable through saliency maps [2] and full gradient representations [39]. However, with the already difficult nature of adversarial learning, which require multiple tricks to even stabilise [12] [37] [7], we argue why create a model with bias to begin with? We relax the assumption that an entire 2D pose is required to predict accurate 3D coordinates, and instead train multiple generators on spatially independent parts of the 2D kinematic skeleton. The knowledge learned is then distilled to an end-to-end model which can predict the 3D coordinates for an entire 2D pose without the bias mentioned previously, giving the framework its name "Teaching Independent Parts Separately" (TIPS). In this paper we build upon [6] and [53] as well as show the stability of our model during training, highlighting that in a truly unsupervised scenario using spatially independent generators would allow for more optimum model to be created, even when no 3D data is accessible. Additionally we introduce three new self-consistency constraints during the adversarial learning cycle which we found to help improve evaluation metrics.

2 Related Work

2.1 3D Human Pose Estimation

There currently exists two main avenues of deep-learning for 3D HPE. The first avenue seeks to learn the mapping of 3D joints directly from a 2D image [32] [22] [27] [21] [40] [41] [42]. The other seeks to build upon the success of 2D pose estimation and learn how to lift a 3D pose from an intermediary 2D pose, with a 2D pose being obtained from an image through techniques such as Stack-Hourglass Architectures [29] or Part Affinity Fields [4]. Our work focuses on the latter 2D to 3D lifting approach which can be organised into the following categories:

2.2 Fully Supervised

Fully supervised approaches seek to learn mappings from paired 2D-3D data which contain ground truth 2D locations of keypoints and their corresponding 3D coordinates. Martinez *et al.* [26] introduced a baseline fully connected regression model which learnt 3D coordinates from their relative 2D locations. Exemplar approaches such as [5] [50] use large dictionaries/databases of 3D poses with a nearest-neighbour search to determine an optimal 3D pose. Jiang *et al.* [17] introduced an exemplar approach that split their 3D dictionary into torso and legs aiming to speed up the nearest-neighbour search process, where as we split up our poses during training to reduce bias and learn a better 3D mapping. Pavllo *et al.* [34] used temporal convolutions over 2D keypoints in order to predict the pose of the central or end frame in a time series, whereas Metha *et al.* [28] utilised multi-task learning to combine a convolutional pose regressor with kinematic skeleton fitting for real

time 3D pose estimation. Luo *et al.* [24] introduced a fully convolutional approach which modelled 3D joint orientations with 2D keypoint detection's. Park *et al.* [31] and Zeng *et al.* [53] introduced the concept of splitting a pose into localised groups during learning, where they assume that an unseen pose may be composed of local joint configurations that appear in different poses within a training set. Unlike our approach however, they still maintain that an entire 2D pose is one independent structure via feature sharing or averaging between localised groups throughout their network. We argue that no feature sharing is required and these localised groups can be assumed as completely independent from one another. Additionally, we distill the knowledge from our sub-networks to an end-to-end network which is both more computationally efficient and our approach better generalises to unseen poses.

2.3 Weakly Supervised

Weakly-Supervised approaches do not use explicit 2D-3D correspondences but either augmented 3D data during training or unpaired 2D-3D data to learn human body priors (shape or articulation). Pavlakos [33] *et al.* and Ronchi *et al.* [36] proposed the learning of 3D poses from 2D with ordinal depth relationships between keypoints (e.g. the right wrist is behind the right elbow). Wandt *et al.* [44] introduced a weakly-supervised adversarial approach which transformed their predicted and ground truth 3D poses into a kinematic space chain prior to being seen by a Wasserstein critic [13]. Yang *et al.* [51] lifted wild 2D poses where no ground truth data is available with a critic network that compared these against existing 3D skeletons. Zhou *et al.* [54] utilised transfer learning, using mixed 2D and 3D labels in a unified network. Drover *et al.* [8] investigated if 3D poses can be learned through 2D self-consistency alone, where they found a 2D pose critic network was also needed.

2.4 Unsupervised

Unsupervised approaches do not utilise any 3D data during training unpaired or otherwise. Kudo *et al.* [19] introduced one of the first unsupervised adversarial networks utilising random re-projections and a 2D critic network, under the assumption that any predicted 3D pose once rotated and reprojected should still produce a believable 2D pose. Chen *et al.* [6] expanded this work and that of [8] by introducing an unsupervised adversarial approach with a self-consistency cycle. They also provided ablation studies highlighting a 7% improvement found when using a temporal cues during training. Yu *et al.* [52] built upon Chen *et al.* [6] highlighting that temporal constraints may hinder a model's performance due to balancing multiple training objectives simultaneously and proposed splitting the problem into both a lifting and scale estimation module. They also found that adding temporal motion consistency can boost the performance of their model by 6%. Similar to [52] we highlight that another issue may lie within the lifting network which could also benefit from being split into two sub-networks.

2.5 Knowledge Distillation

Knowledge distillation is a model compression technique where knowledge is transferred from multiple or one large model (teacher) to a singular small model (student) [14]. Wang *et al.* [45] proposed distilling knowledge from a Non-Rigid Structure from Motion method based on exemplar learning to predict 3D poses. Weinzaepfel *et al.* [47] distilled knowledge from a 3D body, hand and facial pose estimators to a final model to predict the whole-body 3D pose. Their 3D body estimator however still assumed the entire body as one codependent structure during the training which we argue is sub-optimal. Additionally their model requires paired 2D-3D data during training whereas TIPS achieves improved results when trained completely unsupervised. Tripathi *et al.* [43] investigated if knowledge could be distilled across 3D representations, where a teacher network would learn 3D kinematic skeletons from 2D poses, then distill this knowledge to a student network that would predict SMPL [23] representations of 3D poses. Lastly, Xu *et al.* [49] proposed an unsupervised approach where a self-consistent teacher with 2D pose-dictionary based modelling would distill knowledge to a student utilising graphical convolutions to improve estimation accuracy and flexibility.

3 Method

In this section we describe both our adversarial approach to train our 2D to 3D generators, as well as our knowledge distillation approach for our final TIPS model. Our 2D poses consist of N key-points (x_i, y_i) , $i = 1 \dots N$, with the root key-point, the midpoint between the left and right hip joint, being located at the origin $(0, 0)$. Because of the fundamental scale ambiguity associated with monocular images, it is impossible to infer absolute depth from a single view alone [30]. Therefore, we used max-normalisation on each of our 2D poses to scale their 2D coordinates between -1 and 1. This also constrains the range of possible 3D coordinates for these keypoints between -1 and 1, allowing the final function of our generators to be a bounded activation function which helps improve adversarial learning [35]. Though feature selection [15] [48] can be used to find an optimal amount of spatially independent segments to split a 2D pose into, for simplicity we split our pose up into two during training, the torso and legs. Therefore, two generators will be trained using our adversarial approach and one final generator will be trained using knowledge distillation. The full end-to-end training process of our adversarial approach can be seen in Figure 1.

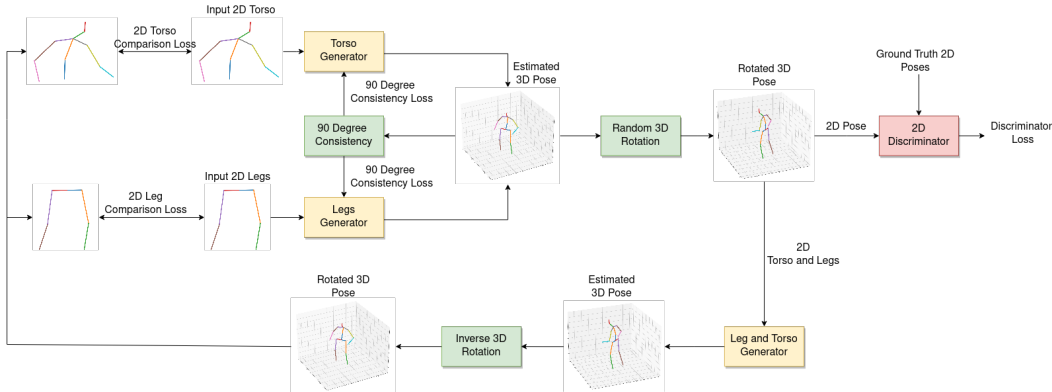


Figure 1: Figure showing the adversarial learning process of the leg and torso generator.

3.1 Generator Architecture

Our generators (G) were fully connected neural networks whose architecture was based on [26] and can be seen in Appendix A.1. These predicted one 3D coordinate for each pair of 2D keypoints:

$$G(x_i, y_i, \mathbf{w}) = \hat{z}_i \quad (1)$$

where \mathbf{w} are the weights of our model learned during training. The torso generator took a vector of 2D keypoints as input consisting of the wrists, elbows, shoulders, neck, spine, head and site keypoint. The leg generator similarly accepted a vector of 2D keypoints consisting of the ankles, knees and hips, with the root keypoint omitted during training as this was a constant. Once both of our generators had made their predictions they were concatenated together and combined with the original 2D keypoints to create our final predicted 3D pose $(\mathbf{x}, \mathbf{y}, \hat{\mathbf{z}})$. Our final TIPS generator by contrast accepted all N keypoints as input and would predict the 3D locations for the full human pose.

3.2 Geometric Consistency Losses

3.2.1 Reprojection Consistency:

Similar to prior work [6] [8] [52], we utilise a self-consistency cycle through random 3D rotations to reproject our predicted 3D poses to new synthetic 2D viewpoints. Let $\mathbf{Y} \in \mathbb{R}^{N \times 2}$ be a matrix containing the 2D keypoints from which our generators will predict. Once a prediction is made and 3D pose obtained, a random rotation matrix \mathbf{R} will be created by uniformly sampling an azimuth angle between $[-\pi, \pi]$ and an elevation angle between $[\frac{-\pi}{18}, \frac{\pi}{18}]$. The predicted 3D pose will be rotated by this matrix and reprojected back into a new synthetic viewpoint, obtaining the new 2D matrix $\tilde{\mathbf{Y}}$. Providing our model is consistent, if we now provide $\tilde{\mathbf{Y}}$ as input to our generators, perform

the inverse rotation of \mathbf{R} on the newly predicted 3D pose and reproject it back into 2D, we should obtain our original matrix of 2D keypoints \mathbf{Y} . This cycle allows our model to learn self-consistency during training where it seeks to minimise the following component in the loss function:

$$L_{2D} = \frac{(\mathbf{Y} - \mathbf{P}(\mathbf{R}^{-1}(\tilde{\mathbf{Y}}_{3D})))^2}{N} \quad (2)$$

Where $\tilde{\mathbf{Y}}_{3D}$ is the 3D pose predicted from $\tilde{\mathbf{Y}}$, \mathbf{P} denotes reprojecting a pose back into 2D and N is the amount of keypoints predicted. Note that as we are training two generators independently from one another, both generators will receive their own L_{2D} loss based on the error between the keypoints that they predicted for. As an example, part of the L_{2D} loss for our torso generator would include the difference between the original 2D keypoint location of the right wrist, and its 2D location once $\tilde{\mathbf{Y}}_{3D}$ was inversely rotated and reprojected. This error would not be included in the L_{2D} loss of the leg generator as it did not predict the 3D location for this keypoint.

3.2.2 90 Degree Consistency

During our study we found that increasing self-consistency was key in reducing the evaluation error (see Appendix A.3). Therefore, we introduce new self-consistency constraints during training based on rotations around the y axis at 90° increments. Let (x, y, \hat{z}) be the predicted 3D pose from our model. If we assume a fixed camera position and rotate our pose 90° , then the depth component of our pose (\hat{z}) prior to rotation will now lie on the x axis from our cameras viewpoint. A visual example of this can be seen in Figure 2.

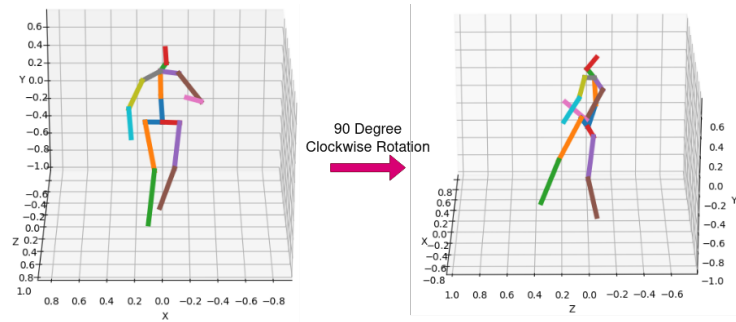


Figure 2: Showing that a 90° rotation of a 3D pose around the y axis with a fixed camera position, will result in the x axis values of the pose prior to rotation representing the z axis values of the pose after the rotation and vice versa.

As we have normalised the axis of our poses between -1 and 1, a 90° clockwise rotation of the 3D pose (x, y, \hat{z}) will produce the pose $(\hat{z}, y, -x)$. Therefore, providing (\hat{z}, y) as input to our generators should result in $-x$ as its predictions. This fact allows for the inclusion of three additional consistency constraints in the loss function of our generators which are as follows:

$$90^\circ \text{ clockwise rotation consistency: } \frac{1}{N} \sum_{i=1}^N (G(\hat{z}_i, y_i) + x_i)^2 = 0 \quad (3)$$

$$90^\circ \text{ counterclockwise rotation consistency: } \frac{1}{N} \sum_{i=1}^N (G(-\hat{z}_i, y_i) - x_i)^2 = 0 \quad (4)$$

$$180^\circ \text{ rotation consistency: } \frac{1}{N} \sum_{i=1}^N (G(x_i, y_i) + G(-x_i, y_i))^2 = 0 \quad (5)$$

These constraints are summed in the final loss function to produce L_{90° . Similar to reprojection consistency, as our generators are making predictions independent from one another, each will receive its own version of L_{90° based on the keypoints that they predicted for. Although we could have included three similar constraints for 90° rotations around the x axis, we found that these hinder the performance of the model. This is due to 90° x axis rotations producing a birds eye and ground up view of a 2D pose, which contain little variance between their 2D keypoints.

3.3 Discriminator Loss

Although self-consistency is important, alone it is not a sufficient enough constraint to generate realistic 3D skeletons [6]. Therefore we utilise a 2D discriminator (D), that takes as input a 2D pose and outputs a value between 0 and 1, representing the probability of the pose being believable. The architecture of our discriminator was a fully connected neural network with the same structure as our generators, but containing one fewer residual blocks and a softmax function in replace of Tanh. It learned to discriminate between the real 2D poses within our data (\mathbf{Y}), and our reprojected 2D pose ($\tilde{\mathbf{Y}}$). This provided feedback to our generators during training, enabling the learning of priors such as joint angles and limb length ratios. Our discriminator utilised the standard GAN loss [11]:

$$\min_{\theta_G} \max_{\theta_D} L_{adv} = \mathbb{E}(\log(D(\mathbf{Y}))) + \mathbb{E}(\log(1 - D(\tilde{\mathbf{Y}}))) \quad (6)$$

Unlike the consistency constraints, we do not provide a unique version of L_{adv} to the torso and leg generator and instead provide the same loss (with a different weight) to both generators. This is due to two reasons; Firstly we wanted our generators to produce a believable pose together which would in turn allow TIPS to produce a believable pose by itself when knowledge was distilled. Having one discriminator see the entire 2D pose would provide this feedback during training. Secondly, we found that multiple discriminators would struggle to provide any useful feedback during training. An example being that 2D legs are normally represented as two straight or bent lines, making it hard for a discriminator to tell apart real from fake.

3.4 Knowledge Distillation

Whilst we believe passing a full pose to a model has an inherent bias and will hamper its performance, the end-to-end process of multiple generators is not as convenient as having one generator which predicts the entire 3D pose. Therefore the final step of our process and the production of our TIPS model is to distill the knowledge of our leg and torso generator to an end-to-end generator. This new generator (G_{TIPS}) will accept the entire 2D pose as input and predict the 3D coordinates of the whole pose. G_{TIPS} was trained to minimise the mean-squared error (MSE) between its own predictions and that of the leg and torso generator as shown:

$$\frac{1}{N} \sum_{i=1}^N (G_{TIPS}(x_i, y_i) - \hat{z}_i)^2 = 0 \quad (7)$$

where \hat{z}_i is the predicted 3D location of the keypoint (x_i, y_i) made by either the leg or torso generator. We use MSE for knowledge distillation as we found that training G_{TIPS} adversarially while including a divergence metric as an additional constraint, would lead to worse performance than if it simply tried to match the leg and torso generators predictions.

3.5 Training

As discussed, our torso and leg generators were trained adversarially with rotational and 90° consistency and our TIPS generator was trained using knowledge distillation. The network parameters are then updated to optimise the total loss for each generator given by:

$$L_{leg} = w_1 L_{adv} + w_2 L_{leg2D} + w_3 L_{leg90^\circ} \quad (8)$$

$$L_{torso} = w_4 L_{adv} + w_2 L_{torso2D} + w_3 L_{torso90^\circ} \quad (9)$$

$$L_{TIPS} = \frac{1}{N} \sum_{i=1}^N (G_{TIPS}(x_i, y_i) - \hat{z}_i)^2 \quad (10)$$

where, $w_1 = 0.05$, $w_2 = 10$, $w_3 = 3$ and $w_4 = 0.08$ are the relative weights for the leg generators adversarial loss, both generators self-consistency loss, both generators 90° consistency loss and torso generators adversarial loss respectively. The discrepancy between w_1 and w_4 was due to how many points each generator predicted. Our torso generator predicted 10 z values out of the 16 in the full

pose, meaning they predicted $\frac{10}{16}$ of the entire pose. Therefore any change in adversarial loss would be more likely due to the torso generator than the leg generator and its weight is higher to reflect this. We trained our model completely unsupervised following [6]. For all models we used a batch size of 8192 and the Adam optimiser with a learning rate of 0.0002. Our experiments use $N = 16$ keypoints. For evaluation we show results of a solo generator as a baseline, both the leg and torso generator working together, and our final TIPS model trained via knowledge distillation.

4 Evaluation and Experiments

4.1 Quantitative Results On Human3.6M

Human3.6M [16] is one of the largest and widely used 3D human pose datasets, containing 3.6 million 3D human poses. It consists of both video and motion capture (MoCap) data from 5 female and 6 male subject, captured from 4 different viewpoints all while the subjects were tasked to perform specific actions (e.g. talking on the phone, taking a photo, eating, etc.). There are two main evaluation protocols for the Human3.6M dataset, which use subjects 1, 5, 6, 7 and 8 for training and subject 9 and 11 for evaluation. Both protocols report the Mean Per Joint Position Error (MPJPE), which is the euclidean distance in millimeters between the predicted and ground truth 3D coordinates. We report the protocol-II performance of our model which employs rigid alignment between the ground truth and predicted pose prior to evaluation. Our results can be seen in Table 1.

As we can see, by interpreting a 2D pose as multiple spatially independent sections for the purpose of 3D pose estimation, we can significantly improve results. This is highlighted by the 18% decrease in MPJPE between TIPS and our baseline solo generator model. TIPS also performed well against several fully supervised models and improved upon [6] which utilised temporal information. Additionally, TIPS managed to achieve the highest performance in both the photo taking and sitting down action as well as joint second highest in the sitting action. By analysing videos of these actions, we believe that TIPS improved these scenarios specifically due to the subjects moving their arms freely throughout the scene but having a fairly neutral stance for their legs (examples of this can be seen in Appendix A.2) highlighting the need for these to be treated as independent from one another.

4.2 Quantitative Results On MPI-INF-3DHP

MPI-INF-3DHP [27] is a markerless MoCap dataset containing the 3D human poses of 8 actors performing 8 different activities. To highlight the generability of TIPS to unseen poses, we show the evaluation results on MPI-INF-3DHP when TIPS is trained on the Human3.6M. The evaluation metrics used are the *percentage of correctly positioned keypoints* (PCK3D) and *area under the curve* (AUC) as defined by [27]. As our predicted poses are normalised, we scale them up by their original normalising factor prior to evaluation. Additionally [44] found there are ambiguities between multiple cameras and 3D pose rotations, causing the potential for inverted predictions as seen in [19]. To remove this ambiguity we assume that the orientation of the pose with respect to the camera is known. Our results can be seen in Table 2.

Comparing tips against [53] we can see that although the PCK at a threshold of 150mm is similar, TIPS has achieved an 11% improvement in AUC (threshold 0mm-150mm). Highlighting that feature sharing between localised groups during training may dampen the generability of a model and that we may achieve improved results by treating them as independent. Similarly TIPS achieves a higher performance than other unsupervised approaches and supervised approaches even when trained on the MPI-INF-3DHP dataset.

4.3 Improved GAN Training Stability

One fundamental question when utilising unsupervised networks is when to stop training. However, we find a lack of information within prior work detailing how long authors have trained their models for. Therefore, we assume that prior work, including ourselves, trained for a set amount of epochs and picked the weights across these epochs which performed best on an evaluation set. Though fine from an evaluation viewpoint, in practice it would not work if we had no ground truth data. In a truly unsupervised scenario there would be three approaches one could use to decide when to stop training. Firstly, we could monitor the discriminators loss and stop training when it too weak or strong. Though there is intuition for this approach, in practice a strong discriminator can cause a

Table 1: Showing the reconstruction error (MPJPE) on Human3.6M. **Legend:** (+) denotes extra data - [51] [33] use 2D annotations from the MPII dataset, [8] increased the amount of Human3.6M training data by 8. (GT) denotes providing 2D ground truth keypoints to a lifting model. (T) denotes the use of temporal information. All results are taking from their respective papers. Lower is better, best in bold, second best underlined.

Method	Approach	Direct.	Discuss	Eat	Greet	Phone	Photo	Posing	Purchase
Martinez <i>et al.</i> [26]	Supervised	39.5	43.2	46.4	47.0	51.0	56.0	41.4	40.6
Pavlo <i>et al.</i> [34] (GT)	Supervised	36.0	<u>38.7</u>	38.0	41.7	40.1	45.9	<u>37.1</u>	35.4
Cai <i>et al.</i> [3] (GT)	Supervised	36.8	38.7	38.2	41.7	40.7	46.8	37.9	35.6
Yang <i>et al.</i> [51] (+)	Weakly-Supervised	26.9	30.9	36.3	39.9	43.9	47.4	28.8	29.4
Pavliakos <i>et al.</i> [33] (+)	Weakly-Supervised	34.7	39.8	41.8	38.6	42.5	47.5	38.0	36.6
Ronchi <i>et al.</i> [36]	Weakly-Supervised	43.6	45.3	45.8	50.9	46.6	55.3	43.3	47.3
Wandt <i>et al.</i> [44] (GT)	Weakly-Supervised	33.6	38.8	32.6	<u>37.5</u>	36.0	44.1	37.8	34.9
Drover <i>et al.</i> [8] (GT)(+)	Weakly-Supervised	33.5	39.3	<u>32.9</u>	37.0	35.8	42.7	39.0	<u>38.2</u>
Kudo <i>et al.</i> [19] (GT)	Unsupervised	125.0	137.9	107.2	130.8	115.1	127.3	147.7	128.7
Chen <i>et al.</i> [6] (T)	Unsupervised	-	-	-	-	-	-	-	-
Solo Generator (Ours)(GT)	Unsupervised	53.3	48.9	56.2	51.6	58.1	47.6	52.8	50.4
Leg and Torso Generator (Ours)(GT)	Unsupervised	38.7	39.6	44.7	44.9	49.4	40.7	46.4	37.2
TIPS (Ours)(GT)	Knowledge Distillation	38.3	39.4	44.7	43.1	48.1	39.7	46.2	37.5

Method	Approach	Sit	SitD	Smoke	Wait	Walk	WalkD.	WalkT.	Avg.
Martinez <i>et al.</i> [26]	Supervised	56.5	69.4	49.2	45.0	49.5	38.0	43.1	47.7
Pavlo <i>et al.</i> [34] (GT)	Supervised	46.8	53.4	41.4	36.9	43.1	30.3	34.8	40.0
Cai <i>et al.</i> [3] (GT)	Supervised	47.6	51.7	41.3	36.8	42.7	31.0	34.7	40.2
Yang <i>et al.</i> [51] (+)	Weakly-Supervised	36.9	58.4	41.5	30.5	29.5	42.5	32.2	37.7
Pavliakos <i>et al.</i> [33] (+)	Weakly-Supervised	50.7	56.8	42.6	39.6	43.9	32.1	36.5	41.8
Ronchi <i>et al.</i> [36]	Weakly-Supervised	56.6	74.3	47.1	48.5	52.1	48.5	49.8	50.3
Wandt <i>et al.</i> [44] (GT)	Weakly-Supervised	39.2	52.0	<u>37.5</u>	39.8	34.1	40.3	34.9	38.2
Drover <i>et al.</i> [8] (GT)(+)	Weakly-Supervised	<u>42.1</u>	52.3	36.9	39.4	36.8	33.2	34.9	<u>38.2</u>
Kudo <i>et al.</i> [19] (GT)	Unsupervised	134.7	139.8	114.5	147.1	130.8	125.6	151.1	130.9
Chen <i>et al.</i> [6] (GT)(T)	Unsupervised	-	-	-	-	-	-	-	51
Solo Generator (Ours)(GT)	Unsupervised	46.7	44.6	49.8	72.7	55.3	49.5	51.5	52.6
Leg and Torso Generator (Ours)(GT)	Unsupervised	39.5	<u>39.4</u>	43.2	54.6	52.0	41.1	45.4	43.8
TIPS (Ours)(GT)	Knowledge Distillation	<u>39.2</u>	39.2	43.3	53.1	51.3	40.5	44.7	43.2

Table 2: Results for the MPI-INF-3DHP dataset. **Legend:** (3DHP) denotes the model being trained on the MPI-INF-3DHP dataset. (H36M) denotes the model being trained on the Human3.6M dataset. (+) denotes additional training data. (*) uses transfer learning during from 2Dposenet. (T) denotes the use of temporal information during training. All results are taking from their respective papers. Higher is better, best in bold, second best underlined.

Method	Approach	PCK	AUC
Mehta <i>et al.</i> [27] (3DHP + H36M)(*)	Supervised	76.5	40.8
Zeng <i>et al.</i> [53] (H36M)	Supervised	77.6	43.8
Yang <i>et al.</i> [51] (H36M)(+)	Weakly-Supervised	69.0	32.0
Wandt <i>et al.</i> [44] (H36M)	Weakly-Supervised	81.8	54.8
Kanazawa <i>et al.</i> [18] (3DHP)	Weakly-Supervised	77.1	40.7
Chen <i>et al.</i> [6] (3DHP)(T)	Unsupervised	71.1	36.3
Kundo <i>et al.</i> [20] (H36M)	Unsupervised	76.5	39.8
Solo Generator (Ours)(H36M)	Unsupervised	75.7	47.0
Leg and Torso Generator (Ours)(H36M)	Unsupervised	77.1	47.9
TIPS (Ours)(H36M)	Knowledge Distillation	<u>78.0</u>	<u>48.8</u>

generator to fail due to vanishing gradients [1] and a weak discriminator provides poor feedback to a generator reducing its performance. Secondly, we could visualise the predictions per epoch and decide by eye which pose is the best. Though having potentially hundreds of epochs and thousands of poses, this is not an efficient solution. Lastly, and more realistically, we could pick the final weight during the training of our model or average the weights between a certain range of epochs to use. For this scenario we show the stability of our leg and torso generators during adversarial training when compared against a solo generator which can be seen in Figure 3.

As shown, by having a leg and torso generator training together not only is the MPJPE lower, but it is stable over a longer period of time. This is especially apparent at epoch 500 where a solo generators error increased drastically before settling around the 70mm mark. Furthermore, these models were trained for 800 epochs. By choosing the last epochs weights to evaluate on the leg

and torso generators average error would have been 45.2mm and the solo generators average error would have been 70.2mm. If we had trained for 400 epochs then the leg and torso generators average error would have been 45.4mm and the solo generators 55.7mm. From epoch 400 to 800 the average error and standard deviation of our leg and torso generator was 45.4 ± 1.1 mm, the average error and standard deviation of a solo generator by comparison was 64.3 ± 6.2 mm. Showing that in a truly unsupervised scenario our model would allow for both better and more consistent results.

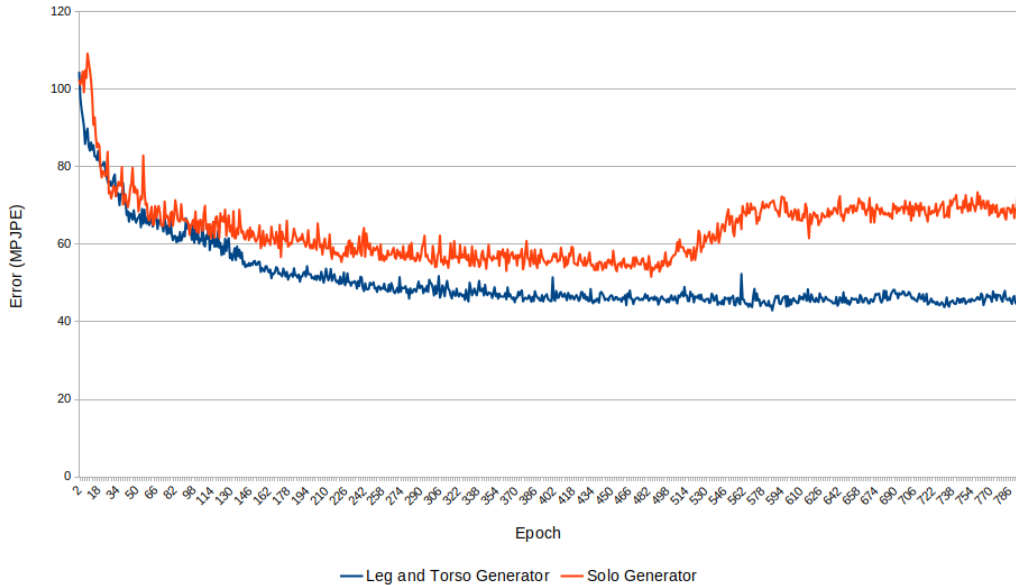


Figure 3: Figure showing the evaluation error (MPJPE) of the leg and torso generators compared against a solo generator on the Human3.6M dataset for each training epoch.

5 Conclusions

This paper presented TIPS, an unsupervised training method for 3D human pose estimation which learns improved 3D poses by learning how to lift independent segments of the 2D kinematic skeleton separately. We proposed using additional constraints to improve the adversarial self-consistency cycle and highlighted that in a truly unsupervised scenario TIPS would allow for a more optimum model to be created through increase GAN stability. By exploiting the spatial independence of the torso and legs we are able to reduce the evaluation error by 18% and although we achieve the best performance in certain actions, we are aware that currently TIPS is unable to completely beat supervised and weakly-supervised approaches. We do believe however that a TIPS training approach may carry over to other supervised and weakly-supervised approaches which could improve their results. Additionally, our high AUC performance in the MPI-INF-3DHP dataset demonstrates that TIPS can generalise well to unseen poses, improving upon prior supervised models that assume a 2D pose should be treated as codependent localised groups.

References

- [1] Martín Arjovsky and Léon Bottou. Towards principled methods for training generative adversarial networks. *ArXiv*, abs/1701.04862, 2017.
- [2] Lennart Brocki and Neo Christopher Chung. Concept saliency maps to visualize relevant features in deep generative models. In *2019 18th IEEE International Conference On Machine Learning And Applications (ICMLA)*, pages 1771–1778, 2019. doi: 10.1109/ICMLA.2019.00287.
- [3] Yujun Cai, Lihao Ge, Jun Liu, Jianfei Cai, Tat-Jen Cham, Junsong Yuan, and Nadia Magnenat Thalmann. Exploiting spatial-temporal relationships for 3d pose estimation via graph convolutional networks. In *2019 IEEE/CVF International Conference on Computer Vision (ICCV)*, pages 2272–2281, 2019. doi: 10.1109/ICCV.2019.00236.

- [4] Z. Cao, G. Hidalgo, T. Simon, S. Wei, and Y. Sheikh. Openpose: Realtime multi-person 2d pose estimation using part affinity fields. *IEEE Transactions on Pattern Analysis and Machine Intelligence*, 43(01):172–186, jan 2021. ISSN 1939-3539. doi: 10.1109/TPAMI.2019.2929257.
- [5] Ching-Hang Chen and Deva Ramanan. 3d human pose estimation = 2d pose estimation + matching. *2017 IEEE Conference on Computer Vision and Pattern Recognition (CVPR)*, pages 5759–5767, 2017.
- [6] Ching-Hang Chen, Amrith Tyagi, Amit Agrawal, Dylan Drover, M. V. Rohith, Stefan Stojanov, and James M. Rehg. Unsupervised 3d pose estimation with geometric self-supervision. *2019 IEEE/CVF Conference on Computer Vision and Pattern Recognition (CVPR)*, pages 5707–5717, 2019.
- [7] Soumith Chintala. How to train a gan (neurips). https://github.com/soumith/talks/blob/master/2016-NIPS/How_To_Train_a_GAN.pdf, 2016. Accessed: 30th March 2022.
- [8] Dylan Drover, Rohith M. V, Ching-Hang Chen, Amit Agrawal, Amrith Tyagi, and Cong Phuoc Huynh. Can 3d pose be learned from 2d projections alone? In Laura Leal-Taixé and Stefan Roth, editors, *Computer Vision – ECCV 2018 Workshops*, pages 78–94, Cham, 2019. Springer International Publishing. ISBN 978-3-030-11018-5.
- [9] Haoshu Fang, Yuanlu Xu, Wenguan Wang, Xiaobai Liu, and Song-Chun Zhu. Learning pose grammar to encode human body configuration for 3d pose estimation. In *AAAI*, 2018.
- [10] David A Forsyth, Okan Arikian, Leslie Ikemoto, Deva Ramanan, and James O’Brien. Computational studies of human motion: Tracking and motion synthesis. 2006.
- [11] Ian Goodfellow, Jean Pouget-Abadie, Mehdi Mirza, Bing Xu, David Warde-Farley, Sherjil Ozair, Aaron Courville, and Yoshua Bengio. Generative adversarial nets. In Z. Ghahramani, M. Welling, C. Cortes, N. Lawrence, and K. Q. Weinberger, editors, *Advances in Neural Information Processing Systems*, volume 27. Curran Associates, Inc., 2014. URL <https://proceedings.neurips.cc/paper/2014/file/5ca3e9b122f61f8f06494c97b1afccf3-Paper.pdf>.
- [12] Ian J. Goodfellow. NIPS 2016 tutorial: Generative adversarial networks. *CoRR*, abs/1701.00160, 2017. URL <http://arxiv.org/abs/1701.00160>.
- [13] Ishaan Gulrajani, Faruk Ahmed, Martin Arjovsky, Vincent Dumoulin, and Aaron C Courville. Improved training of wasserstein gans. In I. Guyon, U. V. Luxburg, S. Bengio, H. Wallach, R. Fergus, S. Vishwanathan, and R. Garnett, editors, *Advances in Neural Information Processing Systems*, volume 30. Curran Associates, Inc., 2017. URL <https://proceedings.neurips.cc/paper/2017/file/892c3b1c6dcd52936e27cbd0ff683d6-Paper.pdf>.
- [14] Geoffrey E. Hinton, Oriol Vinyals, and Jeffrey Dean. Distilling the knowledge in a neural network. *ArXiv*, abs/1503.02531, 2015.
- [15] Yingkun Huang, Weidong Jin, Zhibin Yu, and Bing Li. Supervised feature selection through deep neural networks with pairwise connected structure. *Knowledge-Based Systems*, 204: 106202, 07 2020. doi: 10.1016/j.knosys.2020.106202.
- [16] Catalin Ionescu, Dragos Papava, Vlad Olaru, and Cristian Sminchisescu. Human3.6m: Large scale datasets and predictive methods for 3d human sensing in natural environments. *IEEE Transactions on Pattern Analysis and Machine Intelligence*, 36(7):1325–1339, jul 2014.
- [17] Hao Jiang. 3d human pose reconstruction using millions of exemplars. In *2010 20th International Conference on Pattern Recognition*, pages 1674–1677, 2010. doi: 10.1109/ICPR.2010.414.
- [18] Angjoo Kanazawa, Michael J. Black, David W. Jacobs, and Jitendra Malik. End-to-end recovery of human shape and pose. In *2018 IEEE/CVF Conference on Computer Vision and Pattern Recognition*, pages 7122–7131, 2018. doi: 10.1109/CVPR.2018.00744.
- [19] Yasunori Kudo, Keisuke Ogaki, Yusuke Matsui, and Yuri Odagiri. Unsupervised adversarial learning of 3d human pose from 2d joint locations, 2018.

- [20] Jogendra Nath Kundu, Siddharth Seth, Mayur Rahul, M. Rakesh, Venkatesh Babu Radhakrishnan, and Anirban Chakraborty. Kinematic-structure-preserved representation for unsupervised 3d human pose estimation. In *AAAI*, 2020.
- [21] Sijin Li, Weichen Zhang, and Antoni B. Chan. Maximum-margin structured learning with deep networks for 3d human pose estimation. *International Journal of Computer Vision*, 122: 149–168, 2015.
- [22] Wen-Nung Lie, Guan-Han Lin, Lung-Sheng Shih, Yuling Hsu, Thang Huu Nguyen, and Quynh Nguyen Quang Nhu. Fully convolutional network for 3d human skeleton estimation from a single view for action analysis. In *2019 IEEE International Conference on Multimedia Expo Workshops (ICMEW)*, pages 1–6, 2019. doi: 10.1109/ICMEW.2019.0-120.
- [23] Matthew Loper, Naureen Mahmood, Javier Romero, Gerard Pons-Moll, and Michael J. Black. SMPL: A skinned multi-person linear model. *ACM Trans. Graphics (Proc. SIGGRAPH Asia)*, 34(6):248:1–248:16, October 2015.
- [24] Chenxu Luo, Xiao Chu, and Alan Loddon Yuille. Orinet: A fully convolutional network for 3d human pose estimation. *ArXiv*, abs/1811.04989, 2018.
- [25] D. Luvizon, H. Tabia, and David Picard. Multi-task deep learning for real-time 3d human pose estimation and action recognition. *IEEE transactions on pattern analysis and machine intelligence*, 2020.
- [26] Julieta Martinez, Mir Rayat Imtiaz Hossain, Javier Romero, and J.J. Little. A simple yet effective baseline for 3d human pose estimation. pages 2659–2668, 10 2017. doi: 10.1109/ICCV.2017.288.
- [27] Dushyant Mehta, Helge Rhodin, Dan Casas, Pascal Fua, Oleksandr Sotnychenko, Weipeng Xu, and Christian Theobalt. Monocular 3d human pose estimation in the wild using improved cnn supervision. In *3D Vision (3DV), 2017 Fifth International Conference on*. IEEE, 2017. doi: 10.1109/3dv.2017.00064. URL http://gvv.mpi-inf.mpg.de/3dhp_dataset.
- [28] Dushyant Mehta, Srinath Sridhar, Oleksandr Sotnychenko, Helge Rhodin, Mohammad Shafiei, Hans-Peter Seidel, Weipeng Xu, Dan Casas, and Christian Theobalt. Vnect: Real-time 3d human pose estimation with a single rgb camera. volume 36, 2017. doi: 10.1145/3072959.3073596. URL <http://gvv.mpi-inf.mpg.de/projects/VNect/>.
- [29] Alejandro Newell, Kaiyu Yang, and Jia Deng. Stacked hourglass networks for human pose estimation. In Bastian Leibe, Jiri Matas, Nicu Sebe, and Max Welling, editors, *Computer Vision – ECCV 2016*, pages 483–499, Cham, 2016. Springer International Publishing. ISBN 978-3-319-46484-8.
- [30] Mark Nishimura, David B. Lindell, Christopher Metzler, and Gordon Wetzstein. Disambiguating monocular depth estimation with a single transient. In Andrea Vedaldi, Horst Bischof, Thomas Brox, and Jan-Michael Frahm, editors, *Computer Vision – ECCV 2020*, pages 139–155, Cham, 2020. Springer International Publishing. ISBN 978-3-030-58589-1.
- [31] Sunghoon Park and Nojun Kwak. 3d human pose estimation with relational networks. In *BMVC*, 2018.
- [32] Georgios Pavlakos, Xiaowei Zhou, Konstantinos G. Derpanis, and Kostas Daniilidis. Coarse-to-fine volumetric prediction for single-image 3d human pose. *2017 IEEE Conference on Computer Vision and Pattern Recognition (CVPR)*, pages 1263–1272, 2017.
- [33] Georgios Pavlakos, Xiaowei Zhou, and Kostas Daniilidis. Ordinal depth supervision for 3d human pose estimation. pages 7307–7316, 06 2018. doi: 10.1109/CVPR.2018.00763.
- [34] Dario Pavlo, Christoph Feichtenhofer, David Grangier, and Michael Auli. 3d human pose estimation in video with temporal convolutions and semi-supervised training. pages 7745–7754, 06 2019. doi: 10.1109/CVPR.2019.00794.
- [35] Alec Radford, Luke Metz, and Soumith Chintala. Unsupervised representation learning with deep convolutional generative adversarial networks. *CoRR*, abs/1511.06434, 2016.

- [36] Matteo Ruggero Ronchi, Oisín Mac Aodha, Robert Eng, and Pietro Perona. It’s all relative: Monocular 3d human pose estimation from weakly supervised data. In *British Machine Vision Conference 2018, BMVC 2018, Northumbria University, Newcastle, UK, September 3-6, 2018*, page 300, 2018. URL <http://bmvc2018.org/contents/papers/0182.pdf>.
- [37] Tim Salimans, Ian Goodfellow, Wojciech Zaremba, Vicki Cheung, Alec Radford, Xi Chen, and Xi Chen. Improved techniques for training gans. In D. Lee, M. Sugiyama, U. Luxburg, I. Guyon, and R. Garnett, editors, *Advances in Neural Information Processing Systems*, volume 29. Curran Associates, Inc., 2016. URL <https://proceedings.neurips.cc/paper/2016/file/8a3363abe792db2d8761d6403605aeb7-Paper.pdf>.
- [38] Shibani Santurkar, Dimitris Tsipras, Andrew Ilyas, and Aleksander Madry. How does batch normalization help optimization? In S. Bengio, H. Wallach, H. Larochelle, K. Grauman, N. Cesa-Bianchi, and R. Garnett, editors, *Advances in Neural Information Processing Systems*, volume 31. Curran Associates, Inc., 2018. URL <https://proceedings.neurips.cc/paper/2018/file/905056c1ac1dad141560467e0a99e1cf-Paper.pdf>.
- [39] Suraj Srinivas and François Fleuret. Full-gradient representation for neural network visualization. In *NeurIPS*, 2019.
- [40] X. Sun, J. Shang, S. Liang, and Y. Wei. Compositional human pose regression. In *2017 IEEE International Conference on Computer Vision (ICCV)*, pages 2621–2630, Los Alamitos, CA, USA, oct 2017. IEEE Computer Society. doi: 10.1109/ICCV.2017.284. URL <https://doi.ieeecomputersociety.org/10.1109/ICCV.2017.284>.
- [41] Bugra Tekin, Isinsu Katircioglu, Mathieu Salzmann, Vincent Lepetit, and Pascal Fua. Structured prediction of 3d human pose with deep neural networks. In Edwin R. Hancock Richard C. Wilson and William A. P. Smith, editors, *Proceedings of the British Machine Vision Conference (BMVC)*, pages 130.1–130.11. BMVA Press, September 2016. ISBN 1-901725-59-6. doi: 10.5244/C.30.130. URL <https://dx.doi.org/10.5244/C.30.130>.
- [42] D Tome, Christopher Russell, and L Agapito. Lifting from the deep: Convolutional 3d pose estimation from a single image, 2017.
- [43] S. Tripathi, S. Ranade, A. Tyagi, and A. Agrawal. Posenet3d: Learning temporally consistent 3d human pose via knowledge distillation. In *2020 International Conference on 3D Vision (3DV)*, pages 311–321, Los Alamitos, CA, USA, nov 2020. IEEE Computer Society. doi: 10.1109/3DV50981.2020.00041. URL <https://doi.ieeecomputersociety.org/10.1109/3DV50981.2020.00041>.
- [44] Bastian Wandt and Bodo Rosenhahn. Repnet: Weakly supervised training of an adversarial reprojection network for 3d human pose estimation. In *2019 IEEE/CVF Conference on Computer Vision and Pattern Recognition (CVPR)*, pages 7774–7783, 2019. doi: 10.1109/CVPR.2019.00797.
- [45] Chaoyang Wang, Chen Kong, and Simon Lucey. Distill knowledge from nrsfm for weakly supervised 3d pose learning. *2019 IEEE/CVF International Conference on Computer Vision (ICCV)*, pages 743–752, 2019.
- [46] Jinbao Wang, Shujie Tan, Xiantong Zhen, Shuo Xu, Feng Zheng, Zhenyu He, and Ling Shao. Deep 3d human pose estimation: A review. *Computer Vision and Image Understanding*, 210:103225, 2021. ISSN 1077-3142. doi: <https://doi.org/10.1016/j.cviu.2021.103225>. URL <https://www.sciencedirect.com/science/article/pii/S1077314221000692>.
- [47] Philippe Weinzaepfel, Romain Brégier, Hadrien Combaluzier, Vincent Leroy, and Grégory Rogez. Dope: Distillation of part experts for whole-body 3d pose estimation in the wild. In *Computer Vision – ECCV 2020: 16th European Conference, Glasgow, UK, August 23–28, 2020, Proceedings, Part XXVI*, page 380–397, Berlin, Heidelberg, 2020. Springer-Verlag. ISBN 978-3-030-58573-0. doi: 10.1007/978-3-030-58574-7_23. URL https://doi.org/10.1007/978-3-030-58574-7_23.

- [48] Maksymilian Wojtas and Ke Chen. Feature importance ranking for deep learning. In *Advances in Neural Information Processing Systems 33*, Advances in Neural Information Processing Systems. Morgan Kaufmann Publishers, September 2020. 34th Conference on Neural Information Processing Systems, NeurIPS 2020 ; Conference date: 06-12-2020 Through 12-12-2020.
- [49] Chenxin Xu, Siheng Chen, Maosen Li, and Ya Zhang. Invariant teacher and equivariant student for unsupervised 3d human pose estimation. In *Proceedings of the AAAI Conference on Artificial Intelligence*, volume 35, pages 3013–3021, 2021.
- [50] Jingjing Yang, Lili Wan, Wanru Xu, and Shenghui Wang. 3d human pose estimation from a single image via exemplar augmentation. *Journal of Visual Communication and Image Representation*, 59:371–379, 2019. ISSN 1047-3203. doi: <https://doi.org/10.1016/j.jvcir.2019.01.033>. URL <https://www.sciencedirect.com/science/article/pii/S1047320319300446>.
- [51] Wei Yang, Wanli Ouyang, X. Wang, Jimmy S. J. Ren, Hongsheng Li, and Xiaogang Wang. 3d human pose estimation in the wild by adversarial learning. *2018 IEEE/CVF Conference on Computer Vision and Pattern Recognition*, pages 5255–5264, 2018.
- [52] Zhenbo Yu, Bingbing Ni, Jingwei Xu, Junjie Wang, Chenglong Zhao, and Wenjun Zhang. Towards alleviating the modeling ambiguity of unsupervised monocular 3d human pose estimation. In *Proceedings of the IEEE/CVF International Conference on Computer Vision (ICCV)*, pages 8651–8660, October 2021.
- [53] Ailing Zeng, Xiao Sun, Fuyang Huang, Minhao Liu, Qiang Xu, and Stephen Lin. Srnet: Improving generalization in 3d human pose estimation with a split-and-recombine approach. In Andrea Vedaldi, Horst Bischof, Thomas Brox, and Jan-Michael Frahm, editors, *Computer Vision – ECCV 2020*, pages 507–523, Cham, 2020. Springer International Publishing. ISBN 978-3-030-58568-6.
- [54] Xingyi Zhou, Qixing Huang, Xiao Sun, Xiangyang Xue, and Yichen Wei. Towards 3d human pose estimation in the wild: A weakly-supervised approach. In *The IEEE International Conference on Computer Vision (ICCV)*, Oct 2017.

A Appendix

A.1 Additional Figures

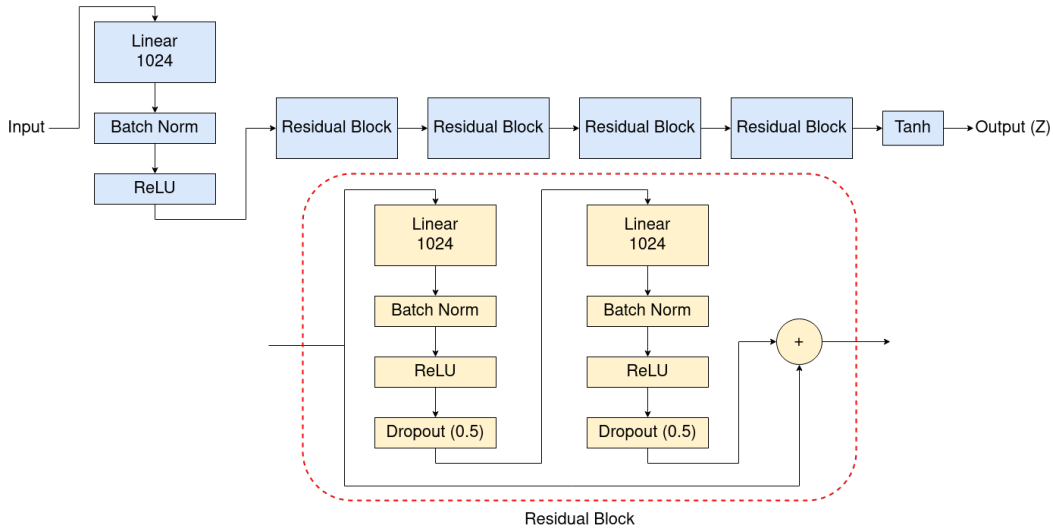


Figure 4: Showing the architecture of the Generators. The network consists of one linear, batch normalisation and activation layer followed by 4 residual blocks. A hyperbolic tangent function would then predict the Z values between -1 and 1.

A.2 Additional Images

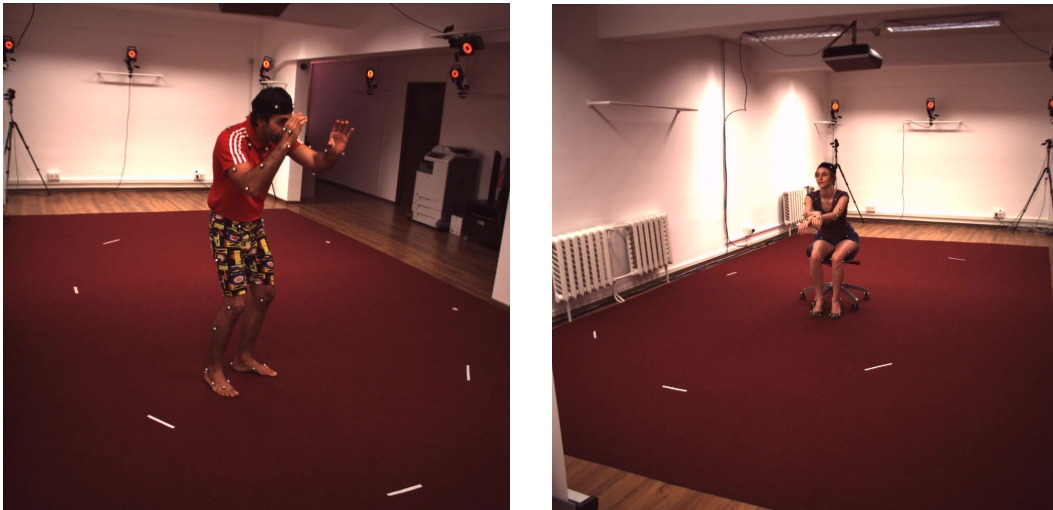


Figure 5: Example images from the Human3.6M dataset showing someone taking a photo (left) and sitting down (right). Note that the arms are performing a specific movement where as the legs in both images are taking a neutral stance for there particular action.

A.3 Improving the consistency cycle

As self-consistency is a constrained optimisation problem even in cases where an unrealistic pose is generated, it is beneficial for this to be low in order to minimise any quantitative error. This can be seen clearly in Table 3 where we see a noticeable decrease in MPJPE between the results in [8] and our recreation with the additional consistency constraints mentioned within our work.

Model	Direct.	Discuss	Eat	Greet	Phone	Photo	Pose	Purchase
Drover <i>et al.</i> [8]	33.5	39.3	32.9	37.0	35.8	42.7	39.0	38.2
Ours (Improved Consistency)	28.3	30.6	37.1	35.7	41.7	33.0	38.1	30.5

Model	Sit	SitDown	Smoke	Wait	Walk	WalkD.	WalkT.	Avg.
Drover <i>et al.</i> [8]	42.1	52.3	36.9	39.4	36.8	33.2	34.9	38.2
Ours (Improved Consistency)	31.1	30.6	33.5	46.2	40.2	32.7	33.9	34.9

Table 3: Table showing the results of [8] and our recreation with additional consistency constraints.

Because of this, we sought to replace the random rotation self-consistency cycle with something more efficient. This was due to a random rotation lending itself to long training times, where the longer a model is trained the more random rotations it will see and therefore the more consistent it will become. However, this could be a problem as highlighted in Figure 3 where a longer training period may lead to GAN instability. By contrast our 90° consistency constraints allows for 3 specified angles of consistency to be learned per training iteration, while also being more computational efficient than randomly rotation a 3D object and re-projecting it. These by themselves however aren't sufficient to learn self-consistency as the model only learns 3 specific angles during training and in the wild many more viewpoints exist. We therefore sought an optimisation formula similar to our 90° consistency that would satisfy all possible viewpoints around the y axis. First let us determine the end position of the points (x_i, y_i, \hat{z}_i) after a random 3D rotation along the y axis:

$$\mathbf{R}(\theta) = \begin{bmatrix} \cos(\theta) & 0 & -\sin(\theta) \\ 0 & 1 & 0 \\ \sin(\theta) & 0 & \cos(\theta) \end{bmatrix} \quad (11)$$

$$\mathbf{R}(\theta) \begin{bmatrix} x_i \\ y_i \\ \hat{z}_i \end{bmatrix} = \begin{bmatrix} x_i \cos(\theta) - \hat{z}_i \sin(\theta) \\ y_i \\ x_i \sin(\theta) + \hat{z}_i \cos(\theta) \end{bmatrix}$$

we substitute these new positions within our original generator function:

$$x_i \sin(\theta) + \hat{z}_i \cos(\theta) = G(x_i \cos(\theta) - \hat{z}_i \sin(\theta), y_i, \mathbf{w}) \quad (12)$$

for $\theta \ll 1$:

$$x_i \theta + \hat{z}_i = G(x_i - \hat{z}_i \theta, y_i, \mathbf{w}) \quad (13)$$

perform Taylor series expansion while ignoring terms of power 2 and above for the small angle θ :

$$x_i \theta + \hat{z}_i = G(x_i, y_i, \mathbf{w}) - \hat{z}_i \theta \frac{\partial}{\partial x_i} G(x_i, y_i, \mathbf{w}) \quad (14)$$

cancel z_i with $G(x_i, y_i, \mathbf{w})$ and remove θ :

$$x_i = -\hat{z}_i \frac{\partial}{\partial x_i} G(x_i, y_i, \mathbf{w}) \quad (15)$$

this leaves us with our final consistency constraint which must be true for all angles:

$$x_i + \hat{z}_i \frac{\partial}{\partial x_i} G(x_i, y_i, \mathbf{w}) = 0 \quad (16)$$

In practice however implementing the above is difficult. This is due to two factors; firstly z_i multiplied by the derivative component provides a Jacobian matrix, which to calculate numerically within current deep learning languages is computationally inefficient, requiring over 100 minutes to train one epoch

on an RTX-8000 GPU. Secondly as we are finding the derivative with respect to the inputs, to maintain gradient independence all batch-norm layers have to be removed from our model as these normalises across the batch dimension. This has the effect of lowering the rate at which our model learns and decreasing its stability while training ([38]).